https://doi.org/10.5194/egusphere-2026-733
Preprint. Discussion started: 25 February 2026

Parameterization of the snow fracture energy to model the onset of crack propagation in snowpack models

Diego Monteiro[1,2,3], Léo Viallon-Galinier[1,2,3], Kévin Fourteau[1,2,3], Oscar Dick[1,2,3], and Pascal Hagenmuller[1,2,3]

[1]Centre d'Études de la Neige, Centre Nationale Recherches Météorologiques (CNRM), Météo-France/CNRS, Grenoble 38000, France
[2]Université Grenoble Alpes, Grenoble 38000, France
[3]Université de Toulouse, Toulouse 31000, France

Correspondence: Diego Monteiro (diego.monteiro@meteo.fr)

Abstract.

Snowpack models are widely used to complement field observations in avalanche risk forecasting. They help estimate key indicators related to dry-snow slab avalanche triggering processes, such as failure initiation and crack propagation. In recent decades, several models have been developed to predict crack propagation propensity, typically characterized by the critical crack length (the cut length beyond which an initial crack self-propagates), measurable in the field using the Propagation Saw Test (PST). However, these models often depend on poorly constrained parameters, particularly, the weak layer fracture energy w_f. In this work, we relate the fracture energy to snow properties that can be measured directly or simulated by detailed snowpack models. To this end, we first exploit microstructural knowledge and data by computing the min-cut on about 300 three-dimensional snow microstructure images. The min-cut represents the smallest ice interface that would need to be fractured to separate two opposing sides of the structure, thus providing a quantitative proxy of fracture energy at the microscale. We fitted a relation between the min-cut and snow properties that can be measured or simulated, namely density and grain morphology. The min-cut is then linearly related to the fracture energy w_f using measurements from Richter et al. (2019), which track weak layers across multiple seasons and sites using PST and observed profiles. We retrieved w_f by inverting the state-of-the-art slab model WEAC (Weißgraeber and Rosendahl, 2023), based on manual measurements and snowpack simulations from the Crocus model. After calibration, w_f is evaluated in two slab models of different complexity for their ability to reproduce observed critical crack lengths, using both observed data and Crocus outputs. Although the correlation between min-cut and w_f remains moderate (i.e. R of 0.5 at most), likely due to measurement and modeling uncertainties, the parameterization demonstrate a clear added-value over the use of a constant w_f in reproducing realistic critical crack lengths (i.e. R = 0.59 and RMSE of 12.5 cm against R = 0.39 and RMSE = 14.5 cm). Moreover, the proposed parameterization performs well for identifying and monitoring weak layers over the course of the season. Its consistent performance across slab models and strong results using Crocus outputs highlight its potential for operational dry-snow slab avalanche hazard monitoring.

https://doi.org/10.5194/egusphere-2026-733
Preprint. Discussion started: 25 February 2026

1 Introduction

Snow avalanches threaten lives and infrastructures in snow-covered mountainous regions (e.g. Techel et al., 2016; Ortner et al., 2025). Accurate avalanche forecasting enables authorities to implement short-term mitigation strategies, such as road closures, evacuations, or deployment of emergency services (e.g. Leone et al., 2014). Forecasting is also important for snow practitioners to choose safer routes and avoid hazardous zones (EAWS, 2026). Observations of snow stratigraphy and stability tests provide valuable information for now-casting avalanche danger. However, these observations are sparse both spatially and temporally due to the time and human resources required for their collection and do not provide any forecast for the next hours and days. To complement these direct measurements, detailed snow models such as Crocus (Vionnet et al., 2012; Lafaysse et al., 2025) and SNOWPACK (Wever et al., 2015) are widely used (Morin et al., 2020). These models simulate the evolution of individual snow layers and their properties, allowing for continuous monitoring of snowpack changes beyond what observations alone can capture. By being forced with numerical weather models, they can forecast future snowpack states, offering spatially and temporally comprehensive predictions essential for avalanche risk assessment.

Assessing the avalanche danger from several simulated snow profiles is not straightforward (Morin et al., 2020). Among loose and slab avalanches, slabs are generally the most dangerous because they mobilize larger snow volumes (McClung and Schaerer, 2006). But they are also the most challenging to predict as their release results from a series of complex mechanisms (Reuter and Schweizer, 2018; Schweizer et al., 2021): failure initiation in a weak layer below a slab, onset of crack propagation, dynamic crack propagation, opening of the tensile crown crack in the slab, and its sliding down the slope. To deliver avalanche-oriented information from snowpack simulations, it is necessary to develop indicators of the likelihood of these mechanisms to occur for a given snow profile.

Among these mechanisms, the onset of crack propagation in the weak layer has been a central topic in avalanche research since the 2000's with the pioneering work of McClung (1979); Van Herwijnen and Jamieson (2005); Gauthier and Jamieson (2008). At the onset of crack propagation, an initiated crack in the weak layer reaches a critical size and begins to self-propagate independently of what initiated it. The propensity of crack to propagate in a certain snow layer can be described by this critical size or more simply by the critical cut length a_c (m) in a conceptual propagation saw test (PST) (Van Herwijnen and Jamieson, 2005; Gauthier and Jamieson, 2006, 2008). A small a_c means that the weak layer below the slab is prone to crack propagation. Modeling of the critical crack length typically relies on linear fracture mechanics and the Griffith criterion (Griffith, 1920; Margolin, 1984). At the onset of crack propagation, the energy release rate of the slab (related to the change of elastic strain energy and gravity potential energy) equals the energy to extend the crack surface area in the weak layer (Heierli et al., 2008). The critical crack length a_c thus depends on both how the slab deforms when it loses support from the weak layer, and the specific fracture energy of the weak layer w_f (J m^{-2}) (Sigrist and Schweizer, 2007).

On one hand, the energy released by the slab during crack propagation can be modeled using beam theory -the slab thickness is generally small compared to the other dimension of the slab or PST snow column- (Heierli et al., 2008; Weißgraeber and Rosendahl, 2023). or simulated using finite elements (Schweizer et al., 2011; Van Herwijnen et al., 2016; Reuter and Schweizer, 2018). In all approaches, the slab energy release is primarily controlled by the slab weight and its effective elastic modulus.

https://doi.org/10.5194/egusphere-2026-733
Preprint. Discussion started: 25 February 2026

Differences between modeling frameworks mainly arise from assumptions regarding boundary conditions (e.g., embedded versus free slab ends in PST configurations), the extent of the simulation domain (e.g., whether deformation energy of the weak layer and the underlying substratum is included), the treatment of potential slab touch-down, and the representation of slab stratigraphy and layering. In contrast, the fracture energy of the weak layer is rarely determined independently. Instead, it is most often inferred a posteriori by inverting the critical crack length measured in PST experiments, using a slab mechanical model fed by the measured or simulated slab stratigraphy (Schweizer et al., 2011; Van Herwijnen et al., 2016; Schweizer et al., 2016b; Adam et al., 2024). An exception is the approach introduced and developed by Reuter et al. (2015); Reuter and Schweizer (2018); Reuter et al. (2019) in which the weak-layer fracture energy w_f is approximated as the minimum penetration resistance integrated over a given length, derived from snow micropenetrometer (SMP) measurements, then used to predict the critical crack length a_c.

To our knowledge, only Gaume et al. (2017); Richter et al. (2019) attempted to parameterize a_c as a function of the layer state variables simulated by a detailed snowpack model, derived from a stress-strength approach using discrete element simulations, different from the classical slab models approach. The proposed parameterization in Richter et al. (2019) offers a practical solution to address the mismatch between the variable describing collapse height (Gaume et al., 2017) and the vertical resolution of the SNOWPACK stratigraphy, using an empirical fit. Richter et al. (2019) show that accounting for the diversity of microstructural properties (i.e. grain size and density) across different weak layers helped better reproduce measured critical crack lengths from simulated profiles. While it does not yet rely on a fully established physical basis, it provides a useful workaround that facilitates model implementation. Furthermore, it currently requires human expertise to pre-identify weak layers.

In summary, forecasting the formation of slab avalanches requires describing the propensity of cracks to propagate in snow layers, which depends on the layer fracture energy w_f. The fracture energy itself is known to be a function of the snow layer density and microstructure (Adam et al., 2024). However, a physically-based and generic parameterization of this fracture energy as a function of simulated layer variables is currently lacking. In this paper, we link w_f to density and grain morphology descriptors that can be simulated by detailed snow models. To do so, we first relate density and grain morphology to the min-cut surface area on 3D images of the snow microstructure. The minimum surface area quantifies the smallest ice interface that would need to be fractured to separate two opposing sides of the microstructure (Hagenmuller et al., 2014). As suggested by LeBaron and Miller (2014), this minimum represents a lower bound for the fracture energy and thus serves as a physical proxy for w_f. Eventually, we scale the simulated min-cut surface area to pseudo-observations of w_f obtained using the state-of-the-art slab models (Weißgraeber and Rosendahl, 2023; Rosendahl and Weissgraeber, 2024) and PST data collected by Richter et al. (2019). All in all, we obtain a relation between density, grain morphology, and weak layer fracture energy. We show that this parameterization helps predict the crack propagation propensity captured by PSTs.

https://doi.org/10.5194/egusphere-2026-733
Preprint. Discussion started: 25 February 2026

2 Materials and Methods

2.1 Slab models

The stability of a snowpack and the critical length above which a crack spontaneously propagates depend on both the fracture energy of the weak layer w_f and on the mechanical behavior of the overlying slab. Therefore, in order to estimate fracture energies from PST or to even predict the critical crack length of a given snowpack stratigraphy, it is necessary to model the deformation of the slab. Specifically, such a model is required to quantify the potential energy (gravity and elastic) released by the slab as it loses basal support from the weak layer during crack propagation. In this work, we used two slab models: the *WEAC* numerical model by Weißgraeber and Rosendahl (2023); Rosendahl and Weissgraeber (2024) and the polynomial model by Heierli et al. (2008). The WEAC model represents the current state-of-the-art and has been used to invert PST results into pseudo-measurements of w_f. Both models are then used to quantify a_c from simulated weak layer fracture energy and slab stratigraphy. In this case, the analytical model by Heierli et al. (2008), despite its simplicity, is particularly valuable due to its computational efficiency, making it well-suited for integration into large-scale simulations such as land surface models.

2.1.1 WEAC model

We employed the python implementation (WEAC package; Rosendahl and Weissgraeber, 2024) of the model described in Weißgraeber and Rosendahl (2023). This model considers the deformation of a multi-layered elastic snow-slab resting on an idealized elastic foundation (Fig. 1.b). The slab can consist of multiple layers with distinct thicknesses, densities and elastic modulus, and the model accounts for bending-extension coupling within the slab. Conditions within the slab and weak layer are chosen to account for the mixed-mode stress conditions (mode I and II). WEAC provides an analytical solution for computing slab displacements, weak layer stress distributions, and energy-release rates. In this study, we used the version 2.5.1 of the WEAC package (Rosendahl and Weissgraeber, 2024). In details, we considered a PST cut upslope (if incline different from 0°) from the right without touchdown (Fig. 1b). The height of the weak layer was set at 3 cm (default value). The elastic modulus E (Pa) of the weak layer is parameterized as a function of weak layer density ρ (either modeled or measured) using Gerling et al. (2017) formulation :

$$E = 6.5 * 10^9 \left(\frac{\rho}{\rho_{ice}} \right)^{5.13} \tag{1}$$

with $\rho_{ice} = 917$ kg m^{-3} the ice density.

https://doi.org/10.5194/egusphere-2026-733
Preprint. Discussion started: 25 February 2026

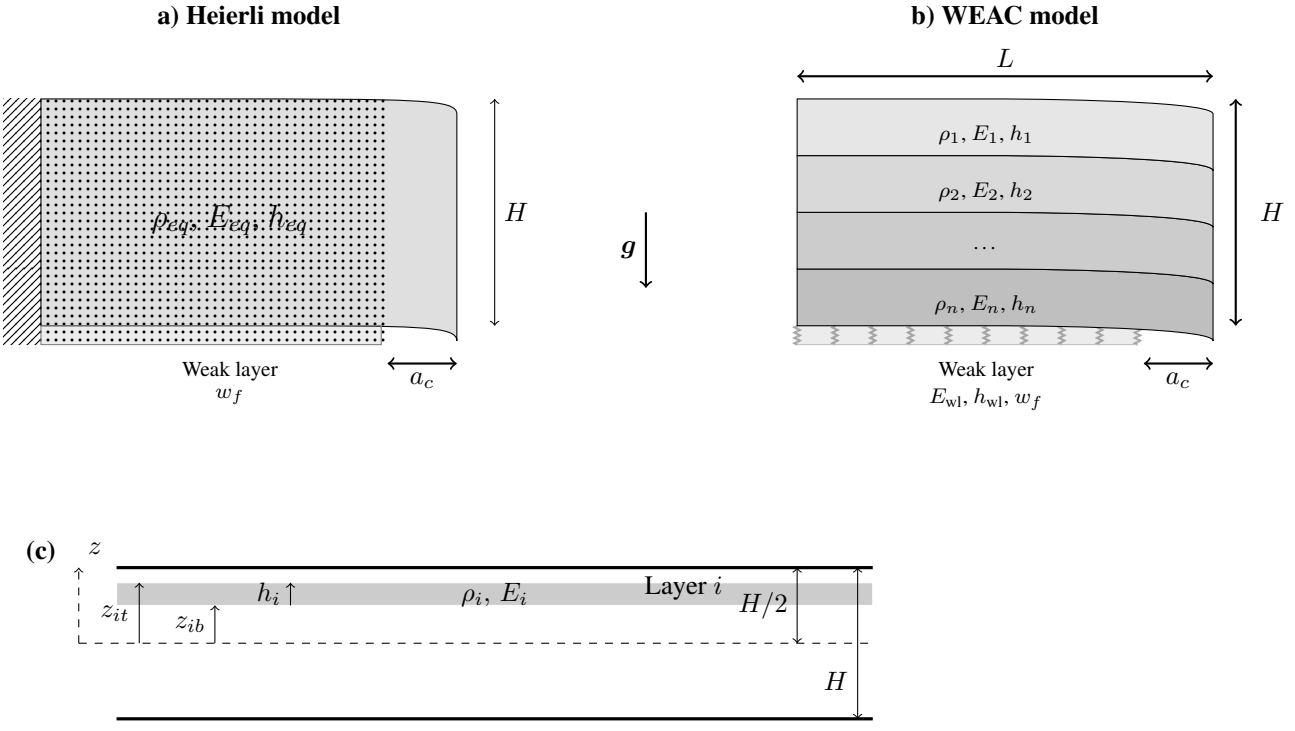

Figure 1. Schematic representation of a) the Heierli model, b) the WEAC model and c) the description of the slab with the variables and reference framework used to calculate the equivalent modulus of elasticity E_{eq}.

2.1.2 Heierli model

The so-called anticrack model was initially developed by Heierli et al. (2008). We used the version described in details by Schweizer et al. (2011). In this model, an homogeneous equivalent slab is represented by a Timoshenko beam fixed on its left side, deforming under its weight and partial absence of basal support (Fig. 1a). The weak layer is assumed to be infinitely stiff and only the elastic strain energy of the overhanging part of the block (above the saw cut) is considered. The model relates the weak layer fracture energy w_f, to the critical crack length a_c and the equivalent slab characteristics: height H, elastic modulus E and density ρ. The slab height H is the sum of the slab layer thicknesses h_i. The slab density is the average slab density $\rho = \frac{\sum \rho_i h_i}{\sum h_i}$. For equivalent elastic modulus of a multi-layered slab, we rely on the same laminate plate theory as in Weißgraeber and Rosendahl (2023). Specifically, we apply equations 8c and 9b of Weißgraeber and Rosendahl (2023), derived for mode I deformation:

$$E = 4\frac{\sum_i E_i(z_{it}^3 - z_{ib}^3)}{H^3} \tag{2}$$

with E_i the young modulus of the layer i, and z_{it} and z_{ib}, respectively, the top and bottom of each layer i as illustrated in Figure 1c). Again, the layer elastic modulus is determined using the density parameterization of Gerling (Eq. 1). It is important to note that this formulation of the equivalent modulus for a multi-layered slab differs from the simpler formulations proposed

https://doi.org/10.5194/egusphere-2026-733
Preprint. Discussion started: 25 February 2026

by Heierli et al. (2008); Schweizer et al. (2011). However, apart from the most complex computation of the equivalent slab modulus, the rest of our implementation directly follows the works of Heierli et al. (2008); Schweizer et al. (2011).

2.2 Snow model: SURFEX-Crocus

SURFEX-Crocus (Vionnet et al., 2012; Masson et al., 2013; Lafaysse et al., 2025) is a coupled system including a land surface model, SURFEX-ISBA (Noilhan and Mahfouf, 1996) with the Crocus snow model (Brun et al., 1992; Vionnet et al., 2012). Crocus belongs to the most detailed class of snow models, including SNOWPACK (Wever et al., 2015). It explicitly models the snowpack stratigraphy and describes the snow microstructure by its density, sphericity and specific surface area. This model was initially developed for local, single-point, simulations in support of the operational forecasting of avalanche hazard in Météo-France. Indeed, its description of the stratigraphy and its layering management enables to follow the evolution of the properties of each layer and, for example, derived indicators of mechanical stability to estimate avalanche risk (Giraud et al., 2002). In this study, we used the version 9.0 of SURFEX-Crocus (Lafaysse et al., 2025).

2.3 Data

2.3.1 Microstructure 3D images and min-cut

Three-dimensional images of snow microstructure were used to compute the minimum cut surface area (min-cut) of various snow samples and to relate it to the snow density and morphology descriptors. We used tomographic data previously measured with X-ray tomography and already binary-segmented. They were gathered from previous studies: Calonne et al. (2011); Hagenmuller et al. (2016, 2019); Peinke et al. (2020); Hagenmuller and Carmagnola (2020); Fourteau et al. (2022); Bernard et al. (2023); Dick et al. (2026). To speed up the computations, the initial cubic images were downscaled by a factor of two, resulting in a voxel size of about 20 μm. The image side length varies between 5 and 12 mm. Each snow image was initially labeled with a snow type according to the international classification (Fierz et al., 2009). In total, 271 snow images were considered.

The min-cut surface area quantifies the smallest ice interface that must be fractured to separate two opposing sides of the microstructure. We used the algorithm of Hagenmuller et al. (2014) with a 26-connectivity to calculate the min-cut surface area in the three Cartesian directions. We normalized the min-cut values by the sample cross-section and retained only the minimal value in the three directions as a fracture energy proxy. For the sake of simplicity, we call, hereafter, this minimal value with no units the *min-cut* and denote it ζ. In addition, the ice fraction ϕ was derived from the 3D images by voxel counting.

2.3.2 Propagation saw tests and observed snow profiles

Two datasets containing propagation saw test measurements and observed snow profiles are used in this study. Both are derived from field campaigns described in detail in Richter et al. (2019). They cover two high elevation sites above Davos, Switzerland: the Weissfluhjoch site (WFJ2; 46.830°N, 9.809°E) located at 2536 m and the Wannengrat site (WAN7; 46.808°N, 9.788°E) located at 2442 m, approximately 3 km apart from the WFJ2 site.

https://doi.org/10.5194/egusphere-2026-733
Preprint. Discussion started: 25 February 2026

Data were collected over three winter seasons, from 2014-2015 to 2016-2017 at site WAN7, and two seasons, from 2015-2016 to 2016-2017 at site WFJ2. During these seasons, a total of seven layers were tested at least once, most of them on a weekly basis for around two months, and for some, several PSTs were carried out on the same date, allowing variability or measurement uncertainties to be taken into account. All of the weak layers were tested at site WAN7, and three of them at both sites. In what follows, they will be referred to using the abbreviation of their grain type according to Fierz et al. (2009) followed by their burial date in year-month-day format (i.e. YYMMDD): FC141216 (WAN7), SH150124 (WAN7), DH151201 (WAN7 and WFJ2), FC151231 (WAN7 and WFJ2), DH161224 (WAN7 and WFJ2).

Propagation saw test (PST) were carried out on isolated columns, 30 cm wide and at least 120 cm long, and on weak layers pre-identified using a compression test (CT). Note that the measured critical crack lengths above 80 cm are removed as they are not considered reliable due to their high values with respect to the PST column length. A total of 61 different critical crack lengths are available at the two field sites, and for each, a complete observed snow profile describing the characteristics of each layer (thickness, density, hand hardness and grain type). For further details concerning the data collection and measurements procedures, please refer to Richter et al. (2019).

2.3.3 Simulated snow stratigraphy using the Crocus snow model

To complement observed snow profiles and assess the applicability of our parameterization of w_f to snow model outputs, we ran SURFEX-Crocus at the two field sites (WAN7 and WFJ2 in Sect. 2.3.2), and matched observed and simulated weak layers.

Both sites are equipped with automatic weather stations that record snow depth, air temperature, relative humidity, wind speed and direction, as well as incoming and outgoing short and long wave radiation. In addition to these variables, the SURFEX-Crocus model requires liquid and solid precipitation fluxes as inputs. For the period when snow is measured on the ground, these variables have been retrieved using the same forcings as in Richter et al. (2019). For the period without snow on the ground (mainly during the mid-June to October periods), the total precipitation that are only measured at the WFJ2 site were applied to both sites and partitioned using a logistic function introduced by Froidurot et al. (2014) :

$$P_{rain} = \frac{1}{1+\exp(\alpha+\beta T_{air}+\gamma RH)} \qquad P_{snow} = 1 - P_{rain} \tag{3}$$

with T_{air} the air temperature, RH the relative humidity and logistic function parameters set as suggested in Froidurot et al. (2014) : $\alpha = 22$, $\beta = -2.7$ and $\gamma = -0.2$. Spin-up simulations were carried out at both sites for seven years, from 2007-08-01 to 2014-08-01, and used as initial conditions for the three-year simulations at WAN7 and WFJ2 sites used in this study. These final simulations are displayed in Fig. 2.

https://doi.org/10.5194/egusphere-2026-733
Preprint. Discussion started: 25 February 2026

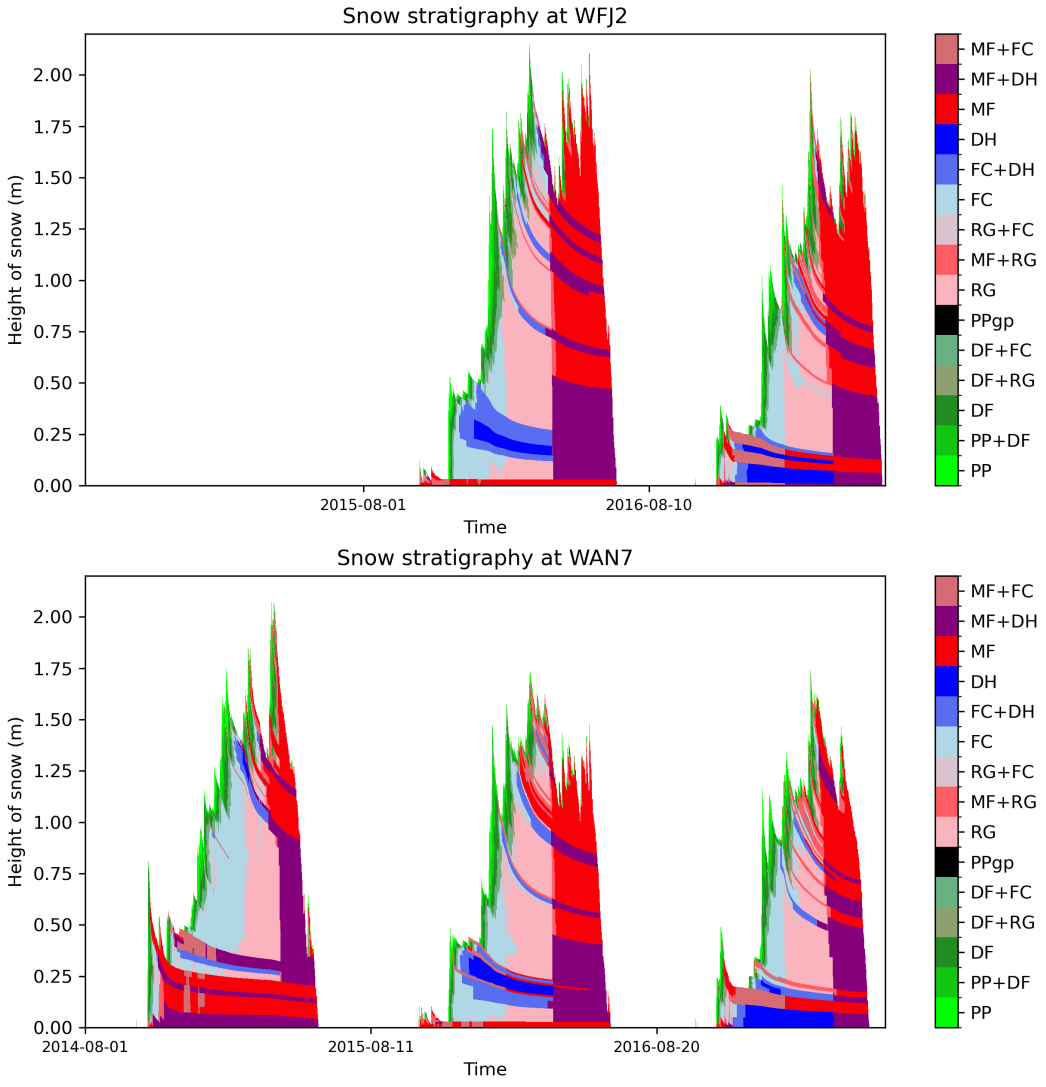

Figure 2. Simulated snow stratigraphy for winters 2015-2016 and 2016-2017 at the Weissflujoch (WFJ2), and for winters 2014-2015, 2015-2016 and 2016-2017 at the Wannengrat (WAN7).

To compare critical crack lengths derived from simulated snow stratigraphy with those measured in the field using PSTs, the corresponding weak layers must be first identified in the simulated profiles. Each observed weak layer is characterized by its burial date, which we used in combination with the deposition date in the Crocus simulations to establish matches. For each weak layer, a time window around the burial date is defined, plus one day and minus one week, to isolate candidate layers in the model. This window is refined if too many layers fall within it. A match is considered satisfactory if the simulated and observed weak layers agree in grain type, burial depth, and surrounding layer characteristics (e.g., crust presence). This approach was

https://doi.org/10.5194/egusphere-2026-733
Preprint. Discussion started: 25 February 2026

successful for all weak layers except SH150124, which the Crocus model could not reproduce. In total, 54 critical crack lengths were retained for comparison.

3 Results

In this section, we first empirically fit the relation between the min-cut derived from 3D images, on one side, and density derived from 3D images and morphology descriptors derived from grain type, on the other side. Then, we estimate the weak layer fracture energy using the PST dataset, the WEAC slab model and the slab stratigraphy (either observed or simulated). With these pseudo-observations, we can relate w_f to the min-cut and ultimately to the density and morphology descriptors. Eventually, we evaluate the parameterization of w_f and its relevance to model the critical crack length in advanced (WEAC) or simple (Heierli) slab models.

3.1 min-cut parameterization using 3D images of snow microstructure

Figure 3 shows the min-cut as a function of the ice volume fraction and grain type. The min-cut increases with ice fraction ϕ, following a power-law relationship. The min-cut theoretically becomes zero below the percolation threshold (i.e. the critical ice fraction at which ice bonds first form a continuous network across the system). Therefore, this power-law relationship, often found for snow properties (e.g. Védrine et al., 2025), must account for a percolation threshold ϕ_t. In addition, for a given density, faceted crystals and depth hoar are characterized by a lower min-cut compared to other grain types. Therefore, an empirical fit should both account for density and grain type. We chose the following multiplicative form:

$$\zeta = f(\text{grain type}) \left(\frac{\phi - \phi_t}{1 - \phi_t} \right)^m \tag{4}$$

with ϕ_t and m parameters to be fitted, and f a scaling factor depending on grain type.

https://doi.org/10.5194/egusphere-2026-733
Preprint. Discussion started: 25 February 2026

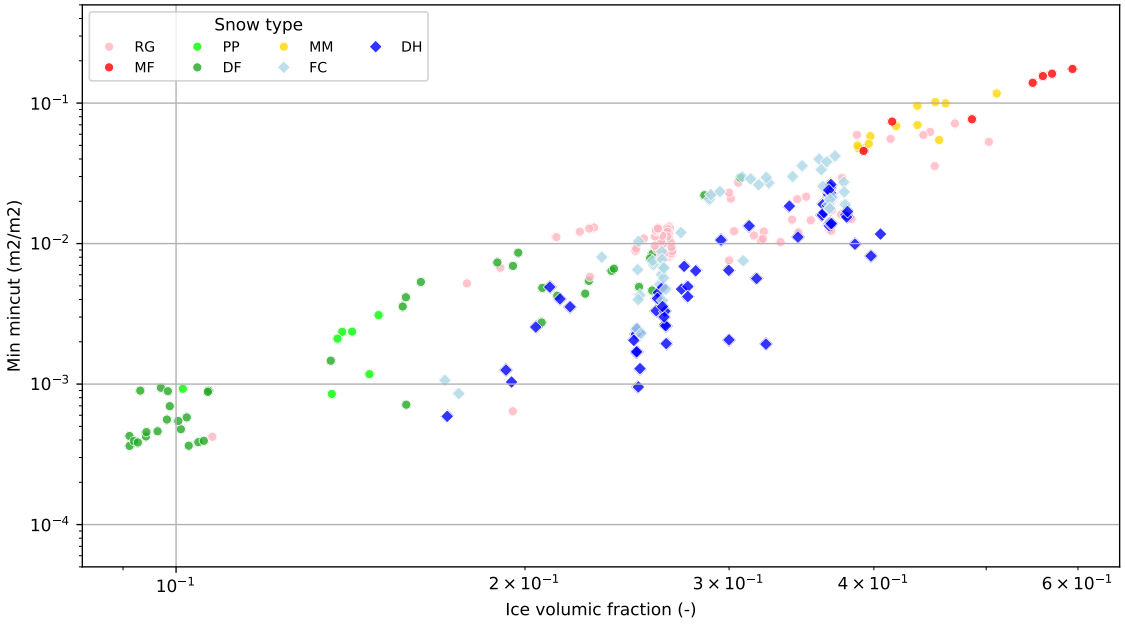

Figure 3. min-cut (m^2/m^2) as a function of the ice volume fraction (-) for all snow samples. Colors are used to differentiate between grain types and typical weak layers grain type are displayed with diamond markers.

To ensure a smooth transition between grain types, the scaling factor f is defined not as a function of the discrete snow types but as a continuous function of the microstructural descriptors used by Crocus to distinguish snow types, namely sphericity Ψ and specific surface area (SSA) s. We used a logistic function for f and expressed the min-cut ζ as:

$$\zeta = \frac{1}{1+\exp(-\alpha_0 - \alpha_\Psi \Psi - \alpha_s s - \alpha_{\Psi s} \Psi s)} \left(\frac{\phi - \phi_t}{1-\phi_t}\right)^m \tag{5}$$

Because grain types are defined along intervals of sphericity and SSA (as reported in Table A1 in appendix), the fitting procedure accounts for these ranges. A least-square minimization yields the following parameters: $\alpha_0 = -2.56$, $\alpha_\Psi = 4.95$, $\alpha_s = 0.14\,\mathrm{kg\ m^{-2}}$, $\alpha_{\Psi s} = -0.30\,\mathrm{kg\ m^{-2}}$, $\phi_t = 0.04$, and $m = 2.46$. Figure 4 shows the fitted relationships (Eq. 5) across the range of sphericity and SSA represented in the Crocus model for three grain types: melt forms (MF), faceted crystals (FC), and depth hoar (DH).

https://doi.org/10.5194/egusphere-2026-733
Preprint. Discussion started: 25 February 2026

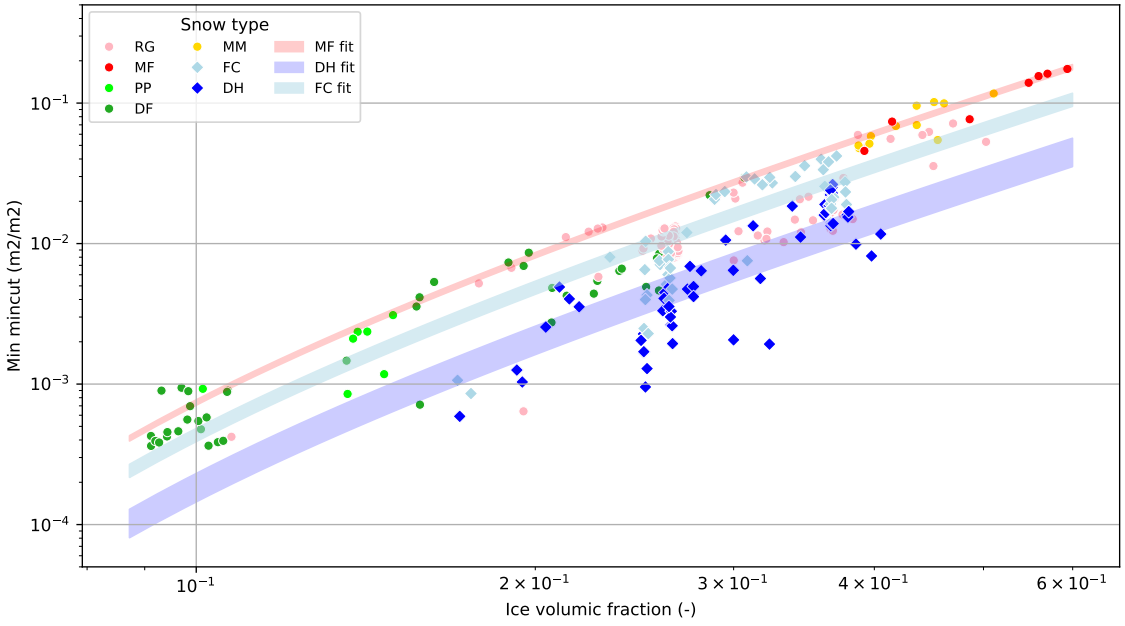

Figure 4. Minimum min-cut (m^2/m^2) as a function of the ice volume fraction (-) for all snow samples. Colors are used to differentiate between grain types and typical weak layers grain type are displayed with diamond markers. The colored shaded areas displays the application of the final parameterization eq. 5, to the range of sphericity and SSA for melt forms (MF) in red, faceted crystals (FC) in light blue and depth hoar (DH) in dark blue.

3.2 Weak layer fracture energy parameterization

In this section, we estimate the relationship between the weak layer fracture energy w_f and the min-cut ζ. Using the WEAC model (Sect. 2.1.1), we invert the critical crack length from PSTs to derive w_f from both observed and simulated snow profiles. These estimates are then compared to the min-cut ζ predicted using Eq. 5. To compute ζ, we used either manually measured density combined with the range of SSA/sphericity values associated to the observed grain type (see table A1 in Appendix A), or the modeled density, SSA and sphericity from the corresponding weak layer in the Crocus profile.

3.2.1 Evaluation of simulated snow stratigraphy

Prior to using the modeled profiles with observed values (i.e., critical crack length from PST), it is necessary to verify that the main characteristics of the stratigraphy are accurately represented in the simulated profiles.

Figure 5 displays the modeled versus measured a) slab density, b) height of the slab, c) weak layer density and d) the weak layer grain types (in the form of a confusion matrix), for each time when PST data are available for both sites and for multiple tested weak layers.

https://doi.org/10.5194/egusphere-2026-733
Preprint. Discussion started: 25 February 2026

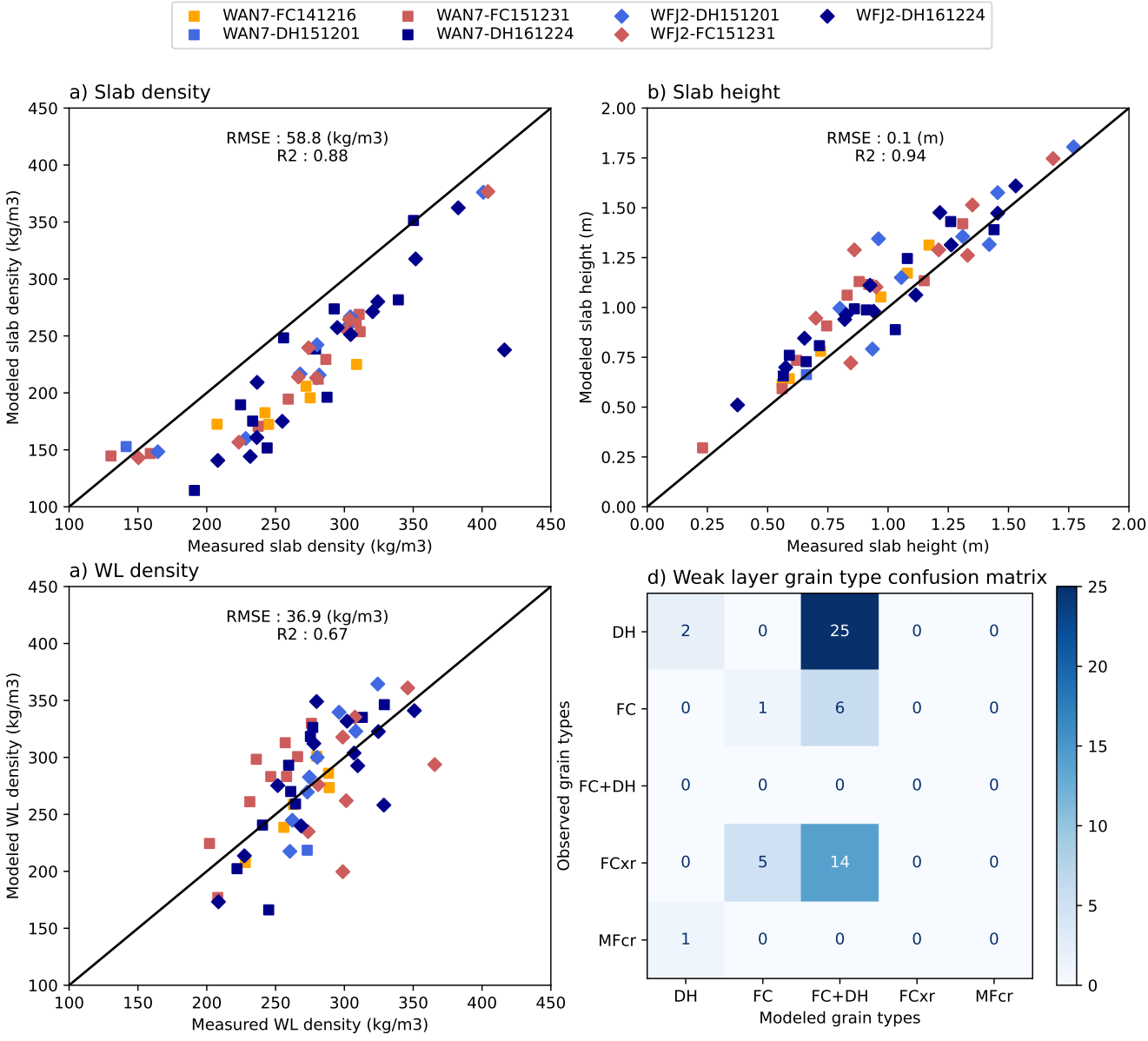

Figure 5. Comparison of (a) modeled to measured mean slab density ρ_{sl}, (b) slab thickness D_{sl}, (c) weak layer density ρ_{wl} and (d) the confusion matrix of the weak layer grain type based on Fierz et al. (2009) nomenclature. Modeled properties were taken from Crocus simulations while measured properties come from manually observed snow profiles. Each colors correspond to a specific tracked weak layer, markers refers to the site of measurement.

Slab density is almost systematically underestimated in the simulated profiles, with a root-mean-square-error ($RMSE$) of 58.8 kg m^{-3}. However, the high linear correlation coefficient (R) of 0.88 indicates that despite systematic errors, Crocus is capable of providing consistent slab densities for all profiles where PSTs were performed. Only one modeled profile (related

https://doi.org/10.5194/egusphere-2026-733
Preprint. Discussion started: 25 February 2026

to the weak layer DH161224 at site WFJ2) appears to be largely underestimated compared to the measurements in terms of slab density, with a measured slab density above 420 kg m^{-3} while the modeled one is below 250 kg m^{-3}.

Unlike slab density, the slab height is mostly slightly overestimated, with a $RMSE$ of 0.1 m. The correlation coefficient with the measured slab height reaches 0.94, which indicates a very consistent agreement.

The modeled densities of the weak layer show greater variability in errors, with no clear trend toward underestimation or overestimation. The $RMSE$ is approximately of 36.9 kg m^{-3}, which is lower than that of slab densities, but with a lower correlation coefficient of 0.67 indicating a more dispersed and less consistent agreement for this variable. This lower agreement is not surprising, given, on the one hand, the difficulty in measuring thin and fragile snow layers, which leads to considerable uncertainty (Proksch et al., 2016), and, on the other hand, modeling errors of snow density and the matching of observed and modeled layers.

As illustrated in Figure 5(d), which shows the correspondence between the measured and modelled grain types at each measurement time and for each weak layer, we note that the majority of the measured weak layers were classified as DH or FC. Similarly, the layers modelled and identified as corresponding in Crocus are also classified as DH, FC or a mix of FC and DH. A significant proportion of the layers designated as DH, FC or FCxr in the observations are found in Crocus as FC+DH (i.e., 45 out of 53 layers), and one layer categorized as MFcr (over which a PST have been performed) is considered as DH in Crocus. These discrepancies can be considered negligible for the purposes of this study, as all these grain types can be considered as weak layer and share similar characteristics.

Overall, the agreement between the measured and modeled characteristics of the slabs and weak layers is satisfactory and very close to that reported in Richter et al. (2019) using the SNOWPACK snow model. Although some systematic errors are present, the simulated profiles are close enough to be used with the measured critical crack length to estimate the weak layer fracture energy using the WEAC model.

3.2.2 Using observed and simulated snow profiles to estimate weak layer fracture energy

The values of w_f based on the observed profiles range between 0.01 and 0.7 J m^{-2}, and correlate weakly with the min-cut estimated using the parameterization Eq. 5 and the measured weak layer densities and snow types (Fig. 6a). The linear correlation coefficients R ranges from 0.31 to 0.36 with a slope between 9.5 and 11.9 J m^{-2}. The use of modeled profiles and modeled weak layer densities leads to values of w_f in the same range but with a better correlation to the min-cut $R = 0.47$, slope of 14.5 J m^{-2}) (Fig. 6Y).

https://doi.org/10.5194/egusphere-2026-733
Preprint. Discussion started: 25 February 2026

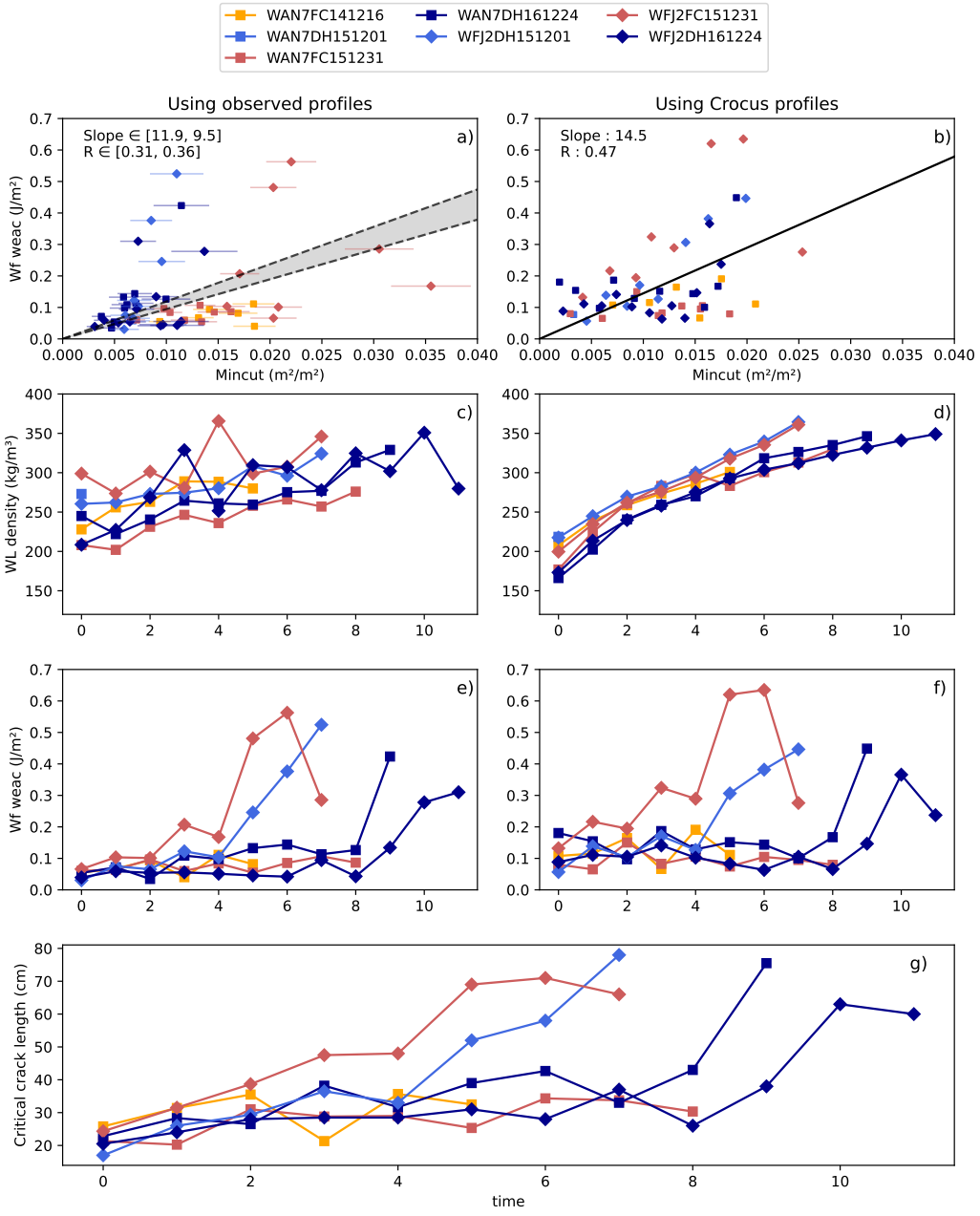

Figure 6. Comparison of the weak layer fracture energy (w_f) obtained using the WEAC model and min-cut using equation 5 determined in section 3.1 applied to observed profiles in the first column (a), c) and e)) and Crocus snow profiles in the second column (b), d) and f)). The colors and markers are associated with each followed weak layer, and the numbering with their evolution over time. For each column, the evolution over time of the weak layer density (c) and d)), the w_f value estimated using the WEAC package (e) and f)), and the measured critical crack length (g)) are also displayed. For observed profiles, slopes, scores and values of min-cut are presented along intervals, corresponding to the intervals of sphericity and SSA for each grain types in table A1.

https://doi.org/10.5194/egusphere-2026-733
Preprint. Discussion started: 25 February 2026

The differences in correlation coefficient between the use of measured and modeled profiles can be explained by the differences in the measured and modeled characteristics of the weak layer and the slab. The measured densities of the weak layer appear to fluctuate significantly over time, as is the case for the "WFJ2-DH161224" and "WFJ2-FC151231" layers (Fig. 6c). For these layers, measurements taken every two weeks may show significant increases in density of around 50 kg m^{-3}, followed by a decrease of the same order at the next measurement. These fluctuations in the density of the weak layer are physically implausible, since over time, under the effect of compaction, most snow layers tend to become denser. They are most likely the result of high measurement uncertainties, further addressed in discussion. The densities of the modeled weak layer follow a quasi-linear monotonic increase over time (Fig. 6d). Since the density of the weak layer is the main variable used to estimate the min-cut in the parameterization Eq. 5, these oscillations may explain some of the differences in correlation found between the use of measured and modeled profiles. In addition to these measurement uncertainties in the weak layer characteristics, there are also uncertainties in the estimation of the PST critical crack lengths (e.g. related to spatial variability of profiles, PST geometries and observers identification of weak layers), used in both cases (i.e. measured and modeled) to invert the WEAC model and obtain w_f.

All in all, assuming a linear relation between w_f and ζ and using Eq. 5, we can express w_f directly as a function of the density, specific surface area, and sphericity of the grains:

$$w_f = \frac{A}{1+\exp(-\alpha_0 - \alpha_\Psi \Psi - \alpha_s s - \alpha_{\Psi s} \Psi s)} \left(\frac{\phi - \phi_t}{1-\phi_t}\right)^m \tag{6}$$

with A = 14.5J m^{-2} for Crocus profiles and A = 9.95J m^{-2} for observed profiles, see section 3.1 eq. 5 for other parameters values.

3.3 Evaluation of modeled critical crack length

In this section, we evaluate the parameterization of the fracture energy w_f (Eq. 6) from several perspectives. First, we assess whether the prediction of the measured a_c is improved by using the proposed parameterization compared to a constant w_f. Next, we analyze the temporal evolution of predicted critical crack lengths from modeled profiles throughout a season. Finally, we examine the potential of predicted critical crack lengths to discriminate between weak layers and more stable layers within a profile.

3.3.1 Comparison of modeled and measured critical crack length

The values of a_c obtained from the measured profiles and a parameterized w_f (Fig. 7a) show an RMSE about 12.5 cm, with a linear correlation coefficient R of 0.59, indicating a good correlation between the measurements and the modeled a_c (Fig. 7a). On this graph, the dispersion of modeled values for small values of a_c (less than 60 cm) is wider than that measured (i.e. 20 to 40 cm versus 15 to 60 cm). In contrast, using a constant w_f instead results in a higher RMSE of 14.5 cm and a lower correlation coefficient of 0.39 (Fig. 7b). Notably, the constant w_f fails to reproduce the observed variability in a_c while the use

https://doi.org/10.5194/egusphere-2026-733
Preprint. Discussion started: 25 February 2026

of a variable w_f better captures the observed variability in a_c, the overall agreement with measurements is improved, though not yet optimal.

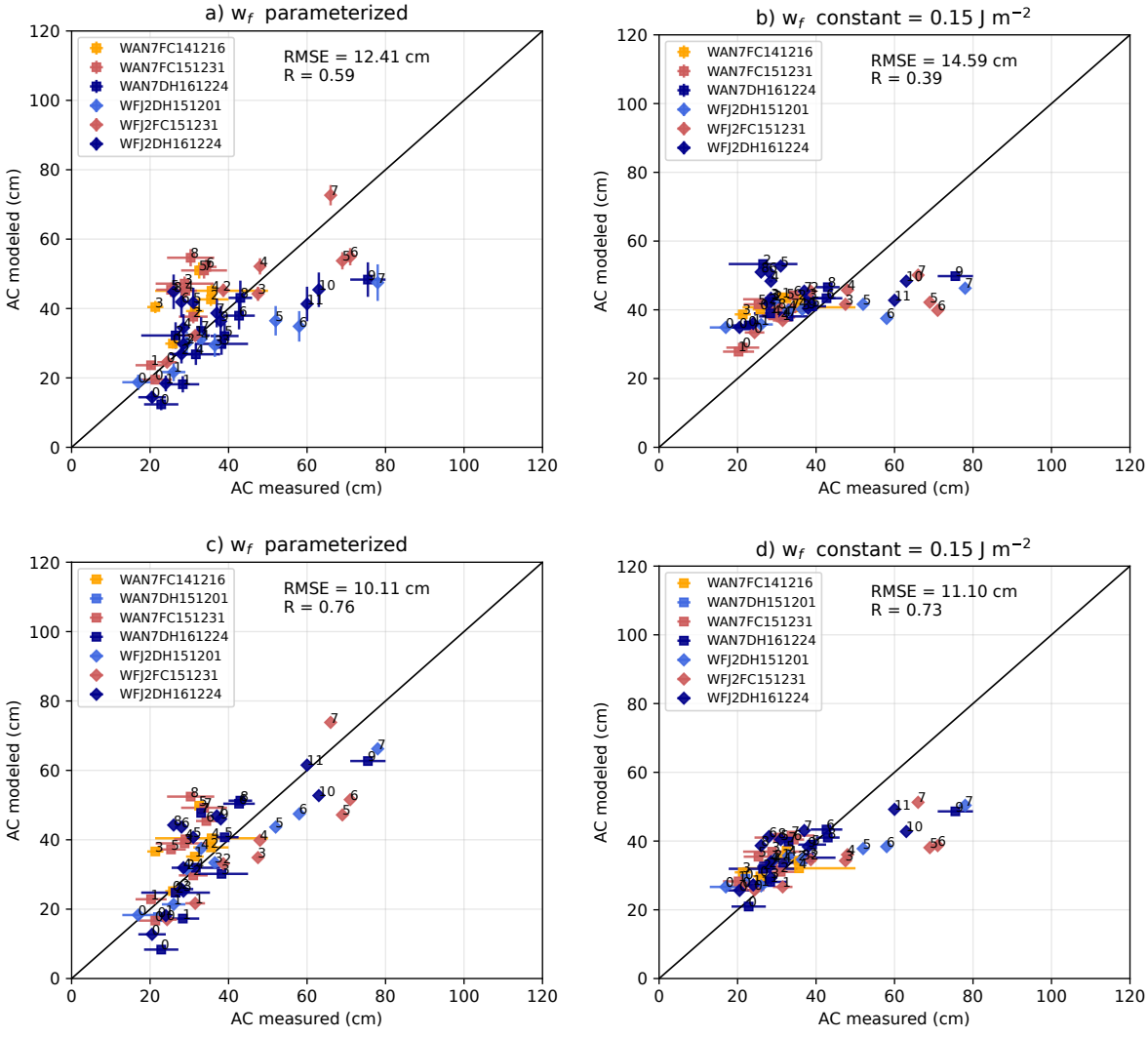

Figure 7. Comparison of the measured and predicted critical crack length a_c for a a weak layer fracture energy w_f either parameterized using Eq. 5 (a, c), or constant (b, d) and different input profiles either observed (a, b) or simulated (c, d). The WEAC model is used to derive a_c. Uncertainties in measured critical crack length are displayed as horizontal error bars, vertical error bars corresponding to the range of a_c values obtained using the intervals of sphericity and SSA (reported in table A1 in appendix) assigned to observed weak layers.

Similar results are found using the modeled profiles (Fig. 7c,d). With a parameterized w_f, the RMSE is 10 cm and the correlation is 0.76— better than with measured profiles. Using a constant w_f slightly degrades the results (RMSE = 11 cm, correlation = 0.73), though the scores remain better than with the parameterized w_f on measured profiles (Fig. 7a). However,

https://doi.org/10.5194/egusphere-2026-733
Preprint. Discussion started: 25 February 2026

predicted a_c values with constant w_f are again strongly bounded, covering a limited range. Surprisingly, using simulated profiles systematically yields better prediction of a_c compared to using observed profiles in the pit the PST were conducted. The possible reasons comprise the measurement uncertainties, in particular that of the weak layer density, whose impact on the estimation of w_f and the min-cut has been shown to be substantial in section 3.2.2.

3.3.2 Time evolution of critical crack length

For each weak layer (except WAN7-DH151201 which was not schematically tracked), we can capture the temporal evolution of the associated a_c along the winter season (Fig. 8). For all time series, the two slab models—Heierli's and WEAC's—exhibit very similar temporal evolutions of a_c, with only minor discrepancies and no systematic bias. The modeled temporal evolution of a_c appears stable over time, showing no oscillations or abrupt peaks that could indicate model instability under certain conditions. This evolution, which is generally increasing, is consistent with observations that all weak layers stabilize over the course of the season.

The values of a_c are most often close to the range of values measured at $\pm$ 10 cm in the field, slightly overestimating it throughout the period for both models, as shown in the layer "WAN7-FC151231," or underestimating it, as in the layer "WJF2-FC151231." The errors are fairly evenly distributed throughout the season, with no systematic errors, and stabilization appears to be captured correctly even in the late season (i.e. end of March, April) for weak layers showing this in the PSTs, such as the "WAN7-DH161224" layer or the "WFJ2-DH151201" layer.

https://doi.org/10.5194/egusphere-2026-733
Preprint. Discussion started: 25 February 2026

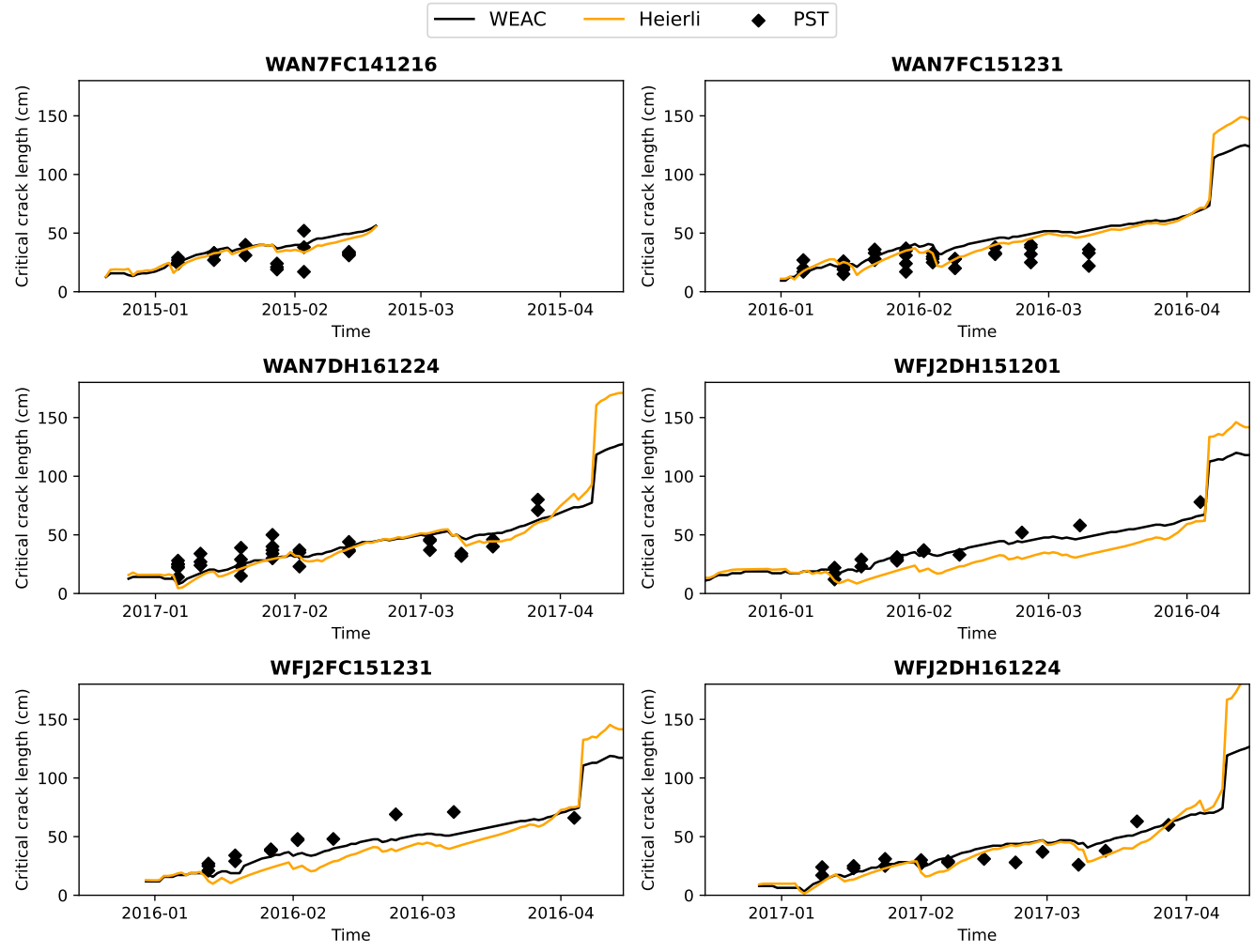

Figure 8. Time series of critical crack length (cm) for each of the weak layers tracked. The black diamonds represent values measured using the PST, and the black and orange lines represent values estimated using the WEAC and Heierli models, respectively, described in sections 2.1.1 and 2.1.2. The two modeled critical crack lengths are calculated using Crocus snow profiles, with the weak layer fracture energy estimated using the linear relationship with the parameterized min-cut (eq 5) established in section 3.2.

3.3.3 Using critical crack length to identify weak layer in snow profiles

Figure 9 shows simulated (left) and measured (right) snow profiles on three dates: January 6, 2015, at site WAN7 in the first column, February 10, 2016, at site WJF2, and March 17, 2017, at site WAN7. These dates were selected to span each season and each site at different times of the winter season.

First, the WEAC and Heierli models predict similar evolution of a_c along a profile (measured or simulated). It is generally minimal near the surface, increasing slowly with depth, with local minimums and maximums generally located in similar areas.

https://doi.org/10.5194/egusphere-2026-733
Preprint. Discussion started: 25 February 2026

These evolution of a_c along the profile is consistent with the fact that near the surface (i.e. and generally early in the season) the layers are not very dense and therefore relatively weak despite the low weight above them. While presenting a low a_c, they are not typically weak layers since the thin and soft slab above is generally too fragile to support the bending induced by the weak layer failure. Deeper down, or later in the season, the layers become denser, even wet, and gain cohesion, becoming for the most part more resistant to failure. However, locally, thin layers with lower resistance due to lower density and/or cohesion may be present. These are the weak layers that are sought after, generally faceted crystals and deep or surface hoar, as these are failure layers found in avalanches (Schweizer et al., 2003; van Herwijnen and Jamieson, 2007) (blue and dark blue colors on the model profiles, square marker and hat on the obs profiles). Note that we focus here solely on one criterion—the crack propagation propensity—and do not account for failure initiation propensity, which may be very low for deeply buried weak layers.

It can be seen that these weak layers are indeed those with the most pronounced local minima of a_c, with the other types of snow surrounding them generally having higher a_c values. These local minima are particularly pronounced at the end of the season, for example in the observed and modeled profile of "WAN7-20170317." They can be seen on the observed profile at depths of 1.10 m, then 0.98 m and 0.35 m, where there are corresponding local minima (i.e., a direct decrease of 10-30 cm in a_c). On the modeled profiles, they are visible at depth of 0.9 m, 0.8 m, 0.5 m, and then 0.15 m. These local minima are also visible to a lesser extent on the WFJ2-20160210 profile at 1.05 m 0.3 m (observed profile) and 1 m and 0.3 m (modeled profile). Ultimately, with the exception of the "FC151231" layer on the observed profile, all of the weak layers tracked and annotated from the measured and modeled profiles stand out as local minima. Although these layers do not constitute absolute minimums across the entire profile (i.e., the top of the profile has lower values), the critical crack length emerges in these examples as a relevant indicator for highlighting weak layers.

https://doi.org/10.5194/egusphere-2026-733
Preprint. Discussion started: 25 February 2026

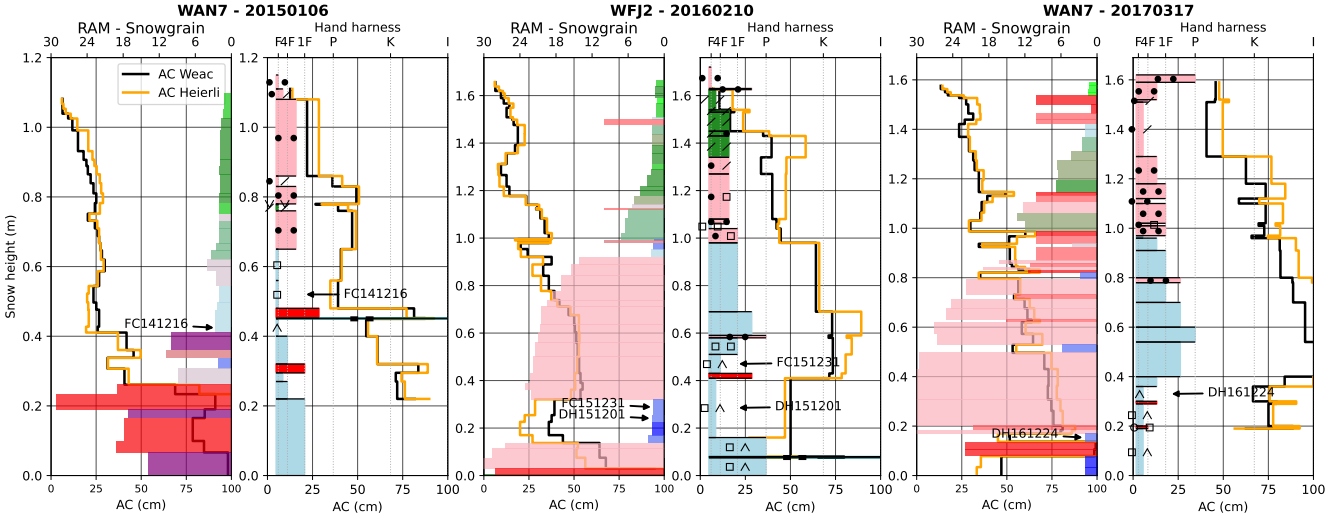

Figure 9. Modeled (left) and observed (right) snow profiles for three dates at different sites: January 6, 2015, and March 17, 2017, at the Wannengrat (WAN7) site, and February 10, 2016, at the Weissflujoch (WFJ2) site. The colors indicate the grain types, and rectangle dimension, the thickness of each layer, their resistance to penetration for the modeled snow profiles, and their hand hardness for the measured snow profiles. For each layer and each profile, the critical crack length using the WEAC and Heierli models is displayed with the weak layer fracture energy estimated using the linear relationship with the parameterized min-cut (eq. 5) established in section 3.2. For each profile, the identified position of the weak layers is displayed either as measured or estimated using the deposition date in the case of modeled snow profiles as described in section 2.3.3.

4 Discussion

4.1 Deriving fracture energy parameterization at layer scale from microscopic measurements of snow samples

We estimated the fracture energy of snow by relating it to simple observable and modelable parameter of snow layers, through a parameterization developed from microstructural properties measured using X-ray microtomography. A central contribution of this work is the use of the min-cut. This approach builds partly on the idea introduced by LeBaron and Miller (2014) and is in line with research seeking to relate macroscopic mechanical variables to microstructural properties derived from micro-tomography. For example, Köchle and Schneebeli (2014) used finite-element simulations and multiple tomographic images to infer macroscopic properties such as the elastic modulus, while Sundu et al. (2024) similarly developed a parameterization of the effective elastic tensor of snow. More recently, Schöttner et al. (2026) combined tomographic images with neural-network methods to predict compressive strength and stiffness. In the present study, we rely on an extensive microtomography dataset covering a broad range of snow types and density, ranging from precipitation particles at around 75 kg m^{-3} to melt forms up to 550 kg m^{-3} as shown in figure 4. This approach avoids the use of discontinuous parameterizations and provides a unified relationship in eq. 6, valid for all snow types. Consequently, this parameterization can be applied consistently across all layers

https://doi.org/10.5194/egusphere-2026-733
Preprint. Discussion started: 25 February 2026

of a snow profile (i.e. either field measured or modeled) to compute w_f. This value can then be incorporated into a slab model to identify the layer most susceptible to crack propagation.

Two key assumptions are made in our approach. First, we assume that the min-cut can be related to a macroscopic quantity, in particular the snow density. Results presented in Section 3.2.2 support this assumption and show that for a given density, layers composed of faceted crystals and depth hoar consistently exhibit lower min-cut values, with depth-hoar layers showing the lowest values among the grain types considered (see figure 3). These observations motivated the introduction of additional microstructural descriptors (grain sphericity and SSA) into the parameterization, such that the min-cut scales depending on grain type and decreases specifically when the grain type approaches the characteristics of faceted crystals and depth hoar. These findings align with Schöttner et al. (2026) results, who show that density captures the first-order variability of mechanical properties such as stiffness and compressive strength, while microstructural attributes are essential for distinguishing the mechanical behavior of persistent weak-layer grain types, including faceted crystals and depth hoar. The second assumption is that the min-cut is linearly related to fracture energy. It appears physically consistent; at the very least, we would expect it to be a lower bound since we neglect any additional energy required to continue fracturing related to the reorganization and stabilization of layers, as well as fractures that would be suboptimal. This hypothesis could not be confirmed, as the linear fit between min-cut and fracture energy provided only a moderate correlation at most (R = 0.47; see figure 6).

Several factors may explain the relatively low correlations obtained in the linear regression between w_f and min-cut, some of which may be related to measurement and modeling uncertainties (discussed in the following section of the discussion), but could also point to a lack of complexity in the proposed parameterization, as the min-cut alone may not fully capture the variability of fracture energy. Nonetheless we demonstrate the clear advantages of using this relationship rather than a constant w_f, as shown by the results in section 3.3.1 and discussed in a further section.

4.2 Measurement and modeling uncertainties

Using modeled rather than measured slab and weak layer characteristics consistently show better performance in the correlation between w_f and the min-cut (Figure 6) and to the R and for RMSE scores for critical crack lengths (Figures 7a-b) and 7c-d)). Lower scores obtained with measured profiles, and the weak correlations between w_f and the min-cut, can partly be attributed to uncertainties in measuring and modeling slab and weak layer properties, primarily density.

The temporal evolution of these properties is shown in Figure 6. While the modeled weak layer density increases smoothly over time, the measured density fluctuates unrealistically by about $\pm$ 50 kg m^{-3} between two-week intervals. These values were obtained using density cutters or tubes (Richter et al., 2019), which are known to have uncertainties up to 10% (i.e. when compared to micro-CT measurements), increasing for layers only a few centimeters thick (concerning most of the followed weak layers), generally overestimating low density and underestimating high density snow layer (Proksch et al., 2016). Added to this uncertainty are the observer's subjective choices regarding the delineation of the different layers, as well as the hectometric variability of the snowpack, all of which make it difficult to monitor the different layers consistently and reliably over the course of a season. Similarly, the evolution of slab characteristics (aggregating all layers) shows greater oscillations in measured than in modeled profiles. Figure 6 also indicates that Crocus densities are systematically lower than measured ones, an

https://doi.org/10.5194/egusphere-2026-733
Preprint. Discussion started: 25 February 2026

already documented model bias such as in Quéno et al. (2016), that could be explained by an underestimation of compaction processes. Critical crack lengths from PSTs, used in both modeled and measured cases, also carry uncertainty, similarly to those related to the weak layer. They result from the observer's choice of cut, spatial metric variability that can be pronounced for thin layers such as weak layers that can be seen on uncertainties in Figures 7, 7 and 8, and by design in the PST protocol for large values approaching the 150 cm column length.

Because the WEAC model depends on numerous parameters (e.g., density, layer thickness, measured critical length), these uncertainties compound, potentially by adding up one another (i.e. underestimating critical length while overestimating weak layer density) thereby applying an increased penalty to the scores.

All of these uncertainties, whether they concern measurements or modeling, make it difficult to estimate a relationship between w_f and the min-cut and probably explain the better scores obtained when using modeled profiles, which, although biased, remain temporally stable and internally consistent. These considerations underline the need for improved field measurement techniques for weak layers and continued refinement of parameter evolution laws in macroscopic snow models.

4.3 On the added-value of the w_f parameterization

The parameterization of w_f remains satisfactory in several respects, even though the correlations between w_f and the min-cut values presented in Section 3.2.2 (Figure 6) are only moderate. First, the values of w_f inferred through inversion of the WEAC model lie between 0.01 and 0.7 J m^{-2} for weak layers. This range is consistent with previous studies, which generally report weak-layer fracture energies between 0.01 and approximately 1.5 J m^{-2} (Schweizer et al., 2011; Bergfeld et al., 2023). This range is also consistent with the total energy release rate values where mode I is dominant (including collapse and in-plane shear), of 0.4–0.8 J m^{-2} as reported in Adam et al. (2024), which was retrieved by performing PSTs over buried surface hoar. This agreement provides confidence that the parameterization derived from our fit will provide physically realistic values of w_f.

Second, the temporal evolution of w_f derived from our simulations is consistent with the observations of Schweizer et al. (2016a), who documented time evolutions of mechanical properties (i.e. elastic modulus and specific fracture energy) in weak layers. Their results show that fracture energy is generally not expected to decrease over time because sintering increases bonding between grains, except under strong temperature-gradient. A similar pattern is visible in figure 6, where many weak layers exhibit relatively stable w_f values around 0.1 J m^{-2} for several weeks before increasing toward the end of the season. This late-season increase is consistent with the stabilization trends described by Schweizer et al. (2016a).

The results in Section 3.3.1, comparing modeled and measured critical crack lengths, further highlight the benefits of using the w_f parameterization developed in Sections 3.1 and 3.2.2, rather than using a constant w_f. For both observed profiles (figures 7) and simulated profiles (figure 7), statistical scores (i.e., R, $RMSE$) are better when the parameterized w_f is used. In addition, employing a constant w_f severely restricts the range of critical crack lengths that the WEAC model can reproduce, preventing any values below 20 cm or above 60 cm. These findings indicate that w_f plays a major role in the dynamics of critical crack length modeling within the WEAC model, and emphasizes the importance of even slight variations during the season, as well as its increase at the end of the season acting the stabilization of the weak layer.

https://doi.org/10.5194/egusphere-2026-733
Preprint. Discussion started: 25 February 2026

Finally, although acceptable scores can still be obtained when using a constant w_f (figure 7), it remains applied to pre-identified weak layers. The narrow range of critical crack lengths produced under a constant w_f would limit the model's applicability for detecting weak layers within full profiles or for tracking their stabilization over time. Overall, these results clearly demonstrate the advantages of using a parameterized w_f over a constant value within the WEAC model.

4.4 Comparing two slab models of different complexity

In the study parts dedicated to the evaluation of the parameterization of w_f, sections 3.3.2 and 3.3.3, two anticrack models of different complexity were compared: Heierli's model and the state-of-the-art WEAC model. The two models differ primarily in their treatment of slab and weak-layer deformation. The WEAC model explicitly accounts for the deformation of a stratified slab as well as that of the weak layer. Its geometry is free on both sides, designed specifically to represent the configuration of a PST. In contrast, the Heierli model relies on a simplified geometry in which a homogeneous slab is embedded on one side, and it focuses on the physical processes occurring at the crack tip. Owing to these simplifications, the Heierli model depends solely on the weak layer fracture energy w_f and does not require additional parameters describing the weak layer that are in any case difficult to obtain through measurements or modeling.

It should be noted that in this study, the Heierli model is implemented using an elastic modulus taken from the recent formulation of Gerling et al. (2017), with an equivalent elastic-modulus expression derived from the mode-I formulation of WEAC (see 2.1.2). These additions enhance the representation of layering effects, even though they are not explicitly included in the deformation model. Such additions are absent from previous implementations described by Heierli et al. (2008); Schweizer et al. (2011); Reuter et al. (2015), and they allow the Heierli model to get results that are more consistent with those of the WEAC model. Despite the differences in complexity and underlying assumptions, the temporal evolution of a_c for weak layers (Figure 8) and the profiles of a_c for selected dates (Figure 9) show similar results for the two models.

Ultimately, although the overall performance of the WEAC model is slightly superior to that of the Heierli model (notably in Figure 8), the discrepancies remain small. This suggests that either model could be used in operational applications based on snow-model outputs, particularly given the relative simplicity of the Heierli formulation and the smaller number of parameters required for its implementation.

5 Conclusions

The principal objective of this study was to establish a framework capable of accurately estimating the sensitivity of any snow layer to crack propagation in a snow profile, with the aim of integrating this capability into macroscopic snow models such as Crocus for improved assessment of dry-snow slab avalanche hazard. A key challenge addressed herein concerns the estimation of parameters that cannot be measured directly, such as the weak layer fracture energy w_f used in slab models like those of Heierli and WEAC (see Section 2.1).

Building upon the state-of-the-art WEAC model and a dataset of nearly 300 tomographic images of diverse snow samples, we developed a new approach to estimate w_f from microstructural properties. First, a power-law relationship was established

https://doi.org/10.5194/egusphere-2026-733
Preprint. Discussion started: 25 February 2026

between bulk snow density and microstructural properties (specifically, the number and size of ice bonds) combined through the min-cut indicator. While most snow types follow a common law, faceted crystals and depth hoar exhibit systematically lower min-cut values. This behavior is captured in the proposed relationship through a scaling coefficient that accounts for grain sphericity and specific surface area. Then, we used a multi-year field dataset from Richter et al. (2019), comprising time series of measured snow stratigraphy and corresponding weak-layer critical crack lengths derived from Propagation Saw Tests (PSTs) across two alpine sites. The continuous min-cut parameterization was compared to fracture energies w_f inverted from the WEAC model using both observed and modeled snow stratigraphies. A moderate correlation between min-cut and w_f was obtained under a linear fit, with improved agreement when modeled stratigraphy (from Crocus) was used. These results are likely the result of both measurement and modeling uncertainties, as well as possible limitations in the explanatory capacity of the min-cut variable alone to fully capture w_f variability.

Despite these limitations, the derived empirical relation between w_f and min-cut provides a consistent parameterization that links macroscopic snow properties (i.e., density, grain sphericity, and SSA) to fracture energy. When reinjected into two anticrack models of differing complexity (WEAC and Heierli), this parameterization significantly improved the prediction of critical crack lengths compared to a constant w_f, reducing errors to 10 cm and achieving linear correlations up to 0.76. Furthermore, the approach demonstrated robust performance in two key aspects: the reliable identification of weak layers within modeled snow profiles, and the realistic temporal evolution of critical crack length over pre-identified weak layers.

Overall, the proposed parameterization represents a step toward bridging microstructural snow physics and macroscopic avalanche forecasting models. Its integration into snowpack models opens up the door to better predicting dry-snow slab avalanches, whether for operational purposes or for assessing hazard evolution under changing climate conditions.

Code and data availability. The WEAC package is available at the zenodo repository Rosendahl and Weissgraeber (2024) and model is extensively described in Weißgraeber and Rosendahl (2023). The SURFEX-Crocus version 9.0 is available at the zenodo repository Lafaysse et al. (2025).Propagation saw tests and observed profiles are attached to the Richter et al. (2019) article. The tomograph-derived parameters (density, grain type and min-cut), SURFEX-Crocus snow simulation and forcing as well as notebook used to produce most figures and analyses are available at the following zenodo repository : Monteiro et al. (2026)

Appendix A

Table A1 associates grain types with sphericity and SSA ranges. These ranges are obtained from the 5th and 95th percentiles of the sphericity and SSA distribution for each grain type, using 60 years of S2M reanalysis (Vernay et al., 2022) in the French Alps massifs using version 9.0 of Crocus snow model (Lafaysse et al., 2025).

https://doi.org/10.5194/egusphere-2026-733
Preprint. Discussion started: 25 February 2026

Grain types	Sphericity intervals	SSA intervals
DF	(0.03, 0.86)	(22.8, 32.6)
DF+FC	(0.0, 0.47)	(16.8, 22.4)
DF+RG	(0.53, 1.0)	(20.0, 25.8)
DH	(0.0, 0.0)	(4.9, 8.9)
FC	(0.0, 0.14)	(14.1, 16.7)
FC+DH	(0.0, 0.26)	(9.4, 13.6)
MF	(0.78, 1.0)	(4.4, 11.1)
MF+DH	(0.69, 1.0)	(4.8, 13.2)
MF+FC	(0.0, 0.45)	(6.6, 16.5)
MF+RF	(0.59, 1.0)	(12.3, 20.4)
PP	(0.36, 0.58)	(44.1, 64.5)
PP+DF	(0.21, 0.68)	(32.4, 42.8)
RG	(0.91, 1.0)	(14.7, 21.7)
RG+FC	(0.22, 0.76)	(13.5, 19.7)
MM	(0.78, 1.0)	(4.4, 11.1)

Table A1. Table of the SSA ($m^2.kg$) and sphericity (-) intervals from Crocus snow model associated with the grain type used in this study.

Author contributions. The study was designed by DM, PH and LV. The formal analysis was performed by DM with input for methodology from PH, LV and KF. OD participates in providing data and analyses. PH handled the funding acquisition for this work, gathered 3D data and computed the min-cut. All authors contributed to the writing of the initial draft.

Competing interests. The authors declare that they have no conflict of interest.

Acknowledgements. The authors would like to thank Benjamin Reuter for the fruitful discussions on the Heierli model and the estimation of w_f, as well as Matthieu Lafaysse and Mathieu Fructus for their help in using the Crocus model to produce snowpack simulations. This work was partly supported by funding from the DGPR (Ministère de la transition écologique, France), contract n°274678.

https://doi.org/10.5194/egusphere-2026-733
Preprint. Discussion started: 25 February 2026

References

Adam, V., Bergfeld, B., Weißgraeber, P., van Herwijnen, A., and Rosendahl, P. L.: Fracture toughness of mixed-mode anticracks in highly porous materials, Nature Communications, 15, 7379, https://doi.org/10.1038/s41467-024-51491-7, 2024.

Bergfeld, B., Van Herwijnen, A., Bobillier, G., Rosendahl, P. L., Weißgraeber, P., Adam, V., Dual, J., and Schweizer, J.: Temporal evolution of crack propagation characteristics in a weak snowpack layer: conditions of crack arrest and sustained propagation, Natural Hazards and Earth System Sciences, 23, 293–315, https://doi.org/10.5194/nhess-23-293-2023, 2023.

Bernard, A., Hagenmuller, P., Montagnat, M., and Chambon, G.: Disentangling creep and isothermal metamorphism during snow settlement with X-ray tomography, Journal of Glaciology, 69, 899–910, https://doi.org/10.1017/jog.2022.109, 2023.

Brun, E., David, P., Sudul, M., and Brunot, G.: A numerical model to simulate snow-cover stratigraphy for operational avalanche forecasting, Journal of Glaciology, 38, 13–22, 1992.

Calonne, N., Flin, F., Morin, S., Lesaffre, B., du Roscoat, S. R., and Geindreau, C.: Numerical and experimental investigations of the effective thermal conductivity of snow, Geophysical research letters, 38, https://doi.org/https://doi.org/10.1029/2011GL049234, 2011.

Dick, O., Calonne, N., Laurent, B., and Hagenmuller, P.: Monitoring dry snow metamorphism using 4D tomography across 20 experimental conditions, Earth System Science Data Discussions, 2026, 1–23, https://doi.org/10.5194/essd-2026-36, 2026.

EAWS: EAWS, https://www.avalanches.org/, 2026.

Fierz, C., Armstrong, R., Durand, Y., Etchevers, P., Greene, E., McClung, D., Nishimura, K., Satyawali, P., Sokratov, S., and der Künste ZHdK, Z.: IACS international classification for seasonal snow on the ground, International Association of Cryospheric Sciences, UNESCO, Paris, 2009.

Fourteau, K., Hagenmuller, P., Roulle, J., and Domine, F.: On the use of heated needle probes for measuring snow thermal conductivity, Journal of Glaciology, 68, 705–719, https://doi.org/10.1017/jog.2021.127, 2022.

Froidurot, S., Zin, I., Hingray, B., and Gautheron, A.: Sensitivity of precipitation phase over the Swiss Alps to different meteorological variables, Journal of Hydrometeorology, 15, 685–696, 2014.

Gaume, J., van Herwijnen, A., Chambon, G., Wever, N., and Schweizer, J.: Snow fracture in relation to slab avalanche release: critical state for the onset of crack propagation, The Cryosphere, 11, 217–228, https://doi.org/10.5194/tc-11-217-2017, 2017.

Gauthier, D. and Jamieson, B.: Towards a field test for fracture propagation propensity in weak snowpack layers, Journal of Glaciology, 52, 164–168, https://doi.org/10.3189/172756506781828962, 2006.

Gauthier, D. and Jamieson, B.: Fracture propagation propensity in relation to snow slab avalanche release: Validating the Propagation Saw Test, Geophysical Research Letters, 35, https://doi.org/https://doi.org/10.1029/2008GL034245, 2008.

Gerling, B., Löwe, H., and van Herwijnen, A.: Measuring the Elastic Modulus of Snow, Geophysical Research Letters, 44, https://doi.org/10.1002/2017GL075110, 2017.

Giraud, G., Navarre, J.-P., and Coléou, C.: Estimation du risque avalancheux dans le système expert MEPRA, 2002.

Griffith, A.: The phenomena of rupture and flow in solids (Philosophical transactions/Royal Society of London ser. A, v. 221), in: Royal Soc, 1920.

Hagenmuller, P. and Carmagnola, C.: Granulométrie de la neige de culture, https://ens.syracuse.cloud/Default/doc/SYRACUSE/70156/granulometrie-de-la-neige-de-culture, num Pages: 10-13, 2020.

Hagenmuller, P., Calonne, N., Chambon, G., Flin, F., Geindreau, C., and Naaim, M.: Characterization of the snow microstructural bonding system through the minimum cut density, Cold Regions Science and Technology, 108, 72–79, 2014.

https://doi.org/10.5194/egusphere-2026-733
Preprint. Discussion started: 25 February 2026

Hagenmuller, P., Matzl, M., Chambon, G., and Schneebeli, M.: Sensitivity of snow density and specific surface area measured by microtomography to different image processing algorithms, The Cryosphere, 10, 1039–1054, https://doi.org/10.5194/tc-10-1039-2016, 2016.

Hagenmuller, P., Flin, F., Dumont, M., Tuzet, F., Peinke, I., Lapalus, P., Dufour, A., Roulle, J., Pézard, L., Voisin, D., Ando, E., Rolland du Roscoat, S., and Charrier, P.: Motion of dust particles in dry snow under temperature gradient metamorphism, The Cryosphere, 13, 2345–2359, https://doi.org/10.5194/tc-13-2345-2019, 2019.

Heierli, J., Gumbsch, P., and Zaiser, M.: Anticrack Nucleation as Triggering Mechanism for Snow Slab Avalanches, Science, 321, 240–243, https://doi.org/10.1126/science.1153948, 2008.

Köchle, B. and Schneebeli, M.: Three-dimensional microstructure and numerical calculation of elastic properties of alpine snow with a focus on weak layers, Journal of Glaciology, 60, 705–713, https://doi.org/10.3189/2014JoG13J220, 2014.

Lafaysse, M., Dumont, M., De Fleurian, B., Fructus, M., Nheili, R., Viallon-Galinier, L., Baron, M., Boone, A., Bouchet, A., Brondex, J., Carmagnola, C., Cluzet, B., Fourteau, K., Haddjeri, A., Hagenmuller, P., Mazzotti, G., Minvielle, M., Morin, S., Quéno, L., Roussel, L., Spandre, P., Tuzet, F., and Vionnet, V.: Version 3.0 of the Crocus snowpack model: source code of implementation within SURFEX and externalized version, https://doi.org/10.5281/zenodo.16943240, 2025.

LeBaron, A. and Miller, D.: An energy-based microstructural constitutive model for fracture in snow, in: Proceedings of the International Snow Science Workshop, pp. 134–138, 2014.

Leone, F., Colas, A., Garcin, Y., Eckert, N., Jomelli, V., and Gherardi, M.: The snow avalanches risk on Alpine roads network. Assessment of impacts and mapping of accessibility loss, Journal of Alpine Research| Revue de géographie alpine, https://doi.org/https://doi.org/10.4000/rga.2501, 2014.

Margolin, L. G.: A generalized Griffith criterion for crack propagation, Engineering fracture mechanics, 19, 539–543, https://doi.org/https://doi.org/10.1016/0013-7944(84)90010-9, 1984.

Masson, V., Le Moigne, P., Martin, E., Faroux, S., Alias, A., Alkama, R., Belamari, S., Barbu, A., Boone, A., Bouyssel, F., Brousseau, P., Brun, E., Calvet, J.-C., Carrer, D., Decharme, B., Delire, C., Donier, S., Essaouini, K., Gibelin, A.-L., Giordani, H., Habets, F., Jidane, M., Kerdraon, G., Kourzeneva, E., Lafaysse, M., Lafont, S., Lebeaupin Brossier, C., Lemonsu, A., Mahfouf, J.-F., Marguinaud, P., Mokhtari, M., Morin, S., Pigeon, G., Salgado, R., Seity, Y., Taillefer, F., Tanguy, G., Tulet, P., Vincendon, B., Vionnet, V., and Voldoire, A.: The SURFEXv7.2 land and ocean surface platform for coupled or offline simulation of earth surface variables and fluxes, Geoscientific Model Development, 6, 929–960, https://doi.org/10.5194/gmd-6-929-2013, 2013.

McClung, D. and Schaerer, P. A.: The avalanche handbook, The Mountaineers Books, 2006.

McClung, D. M.: Shear fracture precipitated by strain softening as a mechanism of dry slab avalanche release, Journal of Geophysical Research: Solid Earth, 84, 3519–3526, 1979.

Monteiro, D., Viallon-Galinier, L., Fourteau, K., Dick, O., and Hagenmuller, P.: meteodmonteir/Article_Wf_param_2026: Replication code and assets, v1.0, submission, https://doi.org/10.5281/zenodo.18505942, 2026.

Morin, S., Horton, S., Techel, F., Bavay, M., Coléou, C., Fierz, C., Gobiet, A., Hagenmuller, P., Lafaysse, M., Ližar, M., Mitterer, C., Monti, F., Müller, K., Olefs, M., Snook, J. S., van Herwijnen, A., and Vionnet, V.: Application of physical snowpack models in support of operational avalanche hazard forecasting: A status report on current implementations and prospects for the future, Cold Regions Science and Technology, 170, 102 910, https://doi.org/https://doi.org/10.1016/j.coldregions.2019.102910, 2020.

Noilhan, J. and Mahfouf, J.-F.: The ISBA land surface parameterisation scheme, Global and Planetary Change, 13, 145–159, 1996.

https://doi.org/10.5194/egusphere-2026-733
Preprint. Discussion started: 25 February 2026

Ortner, G., Michel, A., Kropf, C. M., Bründl, M., and Bresch, D. N.: Assessing the impacts of climate change on snow avalanche-induced risk in alpine regions, Natural Hazards, 121, 10 877–10 904, https://doi.org/https://doi.org/10.1007/s11069-025-07229-9, 2025.

Peinke, I., Hagenmuller, P., Andò, E., Chambon, G., Flin, F., and Roulle, J.: Experimental study of cone penetration in snow using x-ray tomography, Frontiers in Earth Science, 8, 63, https://doi.org/10.3389/feart.2020.00063, 2020.

Proksch, M., Rutter, N., Fierz, C., and Schneebeli, M.: Intercomparison of snow density measurements: bias, precision, and vertical resolution, The Cryosphere, 10, 371–384, https://doi.org/10.5194/tc-10-371-2016, 2016.

Quéno, L., Vionnet, V., Dombrowski-Etchevers, I., Lafaysse, M., Dumont, M., and Karbou, F.: Snowpack modelling in the Pyrenees driven by kilometric-resolution meteorological forecasts, The Cryosphere, 10, 1571–1589, https://doi.org/10.5194/tc-10-1571-2016, 2016.

Reuter, B. and Schweizer, J.: Describing Snow Instability by Failure Initiation, Crack Propagation, and Slab Tensile Support, Geophysical Research Letters, 45, 7019–7027, https://doi.org/10.1029/2018GL078069, 2018.

Reuter, B., Schweizer, J., and van Herwijnen, A.: A process-based approach to estimate point snow instability, The Cryosphere, 9, 837–847, https://doi.org/10.5194/tc-9-837-2015, 2015.

Reuter, B., Proksch, M., Löwe, H., Van Herwijnen, A., and Schweizer, J.: Comparing measurements of snow mechanical properties relevant for slab avalanche release, Journal of Glaciology, 65, 55–67, https://doi.org/10.1017/jog.2018.93, 2019.

Richter, B., Schweizer, J., Rotach, M. W., and van Herwijnen, A.: Validating modeled critical crack length for crack propagation in the snow cover model SNOWPACK, The Cryosphere, 13, 3353–3366, https://doi.org/10.5194/tc-13-3353-2019, 2019.

Rosendahl, P. L. and Weissgraeber, P.: Weak Layer Anticrack Nucleation Model (WEAC), https://doi.org/10.5281/zenodo.11121172, 2024.

Schweizer, J., Bruce Jamieson, J., and Schneebeli, M.: Snow avalanche formation, Reviews of Geophysics, 41, https://doi.org/https://doi.org/10.1029/2002RG000123, 2003.

Schweizer, J., van Herwijnen, A., and Reuter, B.: Measurements of weak layer fracture energy, Cold Regions Science and Technology, 69, 139–144, https://doi.org/10.1016/j.coldregions.2011.06.004, 2011.

Schweizer, J., Reuter, B., van Herwijnen, A., Richter, B., and Gaume, J.: Temporal evolution of crack propagation propensity in snow in relation to slab and weak layer properties, The Cryosphere, 10, 2637–2653, https://doi.org/10.5194/tc-10-2637-2016, 2016a.

Schweizer, J., Reuter, B., Van Herwijnen, A., Richter, B., and Gaume, J.: Temporal evolution of crack propagation propensity in snow in relation to slab and weak layer properties, The Cryosphere, 10, 2637–2653, https://doi.org/10.5194/tc-10-2637-2016, 2016b.

Schweizer, J., Bartelt, P., and van Herwijnen, A.: Chapter 12 - Snow avalanches, in: Snow and Ice-Related Hazards, Risks, and Disasters (Second Edition), edited by Haeberli, W. and Whiteman, C., Hazards and Disasters Series, pp. 377–416, Elsevier, second edition edn., ISBN 978-0-12-817129-5, https://doi.org/https://doi.org/10.1016/B978-0-12-817129-5.00001-9, 2021.

Schöttner, J., Zeller-Plumhoff, B., Hagenmuller, P., Weißgraeber, P., Rosendahl, P. L., Löwe, H., Schweizer, J., and van Herwijnen, A.: The influence of snow microstructure on the compressive mechanical properties of weak snowpack layers, Acta Materialia, 302, 121 657, https://doi.org/https://doi.org/10.1016/j.actamat.2025.121657, 2026.

Sigrist, C. and Schweizer, J.: Critical energy release rates of weak snowpack layers determined in field experiments, Geophysical Research Letters, 34, https://doi.org/https://doi.org/10.1029/2006GL028576, 2007.

Sundu, K., Freitag, J., Fourteau, K., and Löwe, H.: A microstructure-based parameterization of the effective anisotropic elasticity tensor of snow, firn, and bubbly ice, The Cryosphere, 18, 1579–1596, https://doi.org/10.5194/tc-18-1579-2024, 2024.

Techel, F., Jarry, F., Kronthaler, G., Mitterer, S., Nairz, P., Pavšek, M., Valt, M., and Darms, G.: Avalanche fatalities in the European Alps: long-term trends and statistics, Geographica Helvetica, 71, 147–159, https://doi.org/10.5194/gh-71-147-2016, 2016.

https://doi.org/10.5194/egusphere-2026-733
Preprint. Discussion started: 25 February 2026

Van Herwijnen, A. and Jamieson, B.: High-speed photography of fractures in weak snowpack layers, Cold Regions Science and Technology, 43, 71–82, https://doi.org/https://doi.org/10.1016/j.coldregions.2005.05.005, 2005.

van Herwijnen, A. and Jamieson, B.: Snowpack properties associated with fracture initiation and propagation resulting in skier-triggered dry snow slab avalanches, Cold Regions Science and Technology, 50, 13–22, https://doi.org/https://doi.org/10.1016/j.coldregions.2007.02.004, snow and Avalanches EGU 2006, 2007.

Van Herwijnen, A., Gaume, J., Bair, E. H., Reuter, B., Birkeland, K. W., and Schweizer, J.: Estimating the effective elastic modulus and specific fracture energy of snowpack layers from field experiments, Journal of Glaciology, 62, 997–1007, https://doi.org/10.1017/jog.2016.90, 2016.

Védrine, L., Hagenmuller, P., Gélébart, L., Montagnat, M., and Löwe, H.: Sensitivity of the viscoplasticity of polycrystals to porosity and pore-to-crystal size ratio, Acta Materialia, p. 121507, https://doi.org/10.1016/j.actamat.2025.121507, 2025.

Vernay, M., Lafaysse, M., Monteiro, D., Hagenmuller, P., Nheili, R., Samacoïts, R., Verfaillie, D., and Morin, S.: The S2M meteorological and snow cover reanalysis over the French mountainous areas: description and evaluation (1958–2021), Earth System Science Data, 14, 1707–1733, https://doi.org/10.5194/essd-14-1707-2022, 2022.

Vionnet, V., Brun, E., Morin, S., Boone, A., Faroux, S., Moigne, P. L., Martin, E., and Willemet, J.-M.: The detailed snowpack scheme Crocus and its implementation in SURFEX v7. 2, Geoscientific Model Development, 5, 773–791, 2012.

Weißgraeber, P. and Rosendahl, P. L.: A closed-form model for layered snow slabs, The Cryosphere, 17, 1475–1496, https://doi.org/10.5194/tc-17-1475-2023, 2023.

Wever, N., Schmid, L., Heilig, A., Eisen, O., Fierz, C., and Lehning, M.: Verification of the multi-layer SNOWPACK model with different water transport schemes, The Cryosphere, 9, 2271–2293, 2015.